Stress fluctuations in continuously sheared dense granular materials

Piroz Zamankhan and Tero Tynjälä
Department of Energy Technology, Lappeenranta University of Technology, Fin-53851, Lappeenranta, Finland

William Polashenski, Jr.
Lomic, Inc., 200 Innovation Boulevard, State College, Pennsylvania 16803

Parsa Zamankhan and Pertti Sarkomaa
Department of Energy Technology, Lappeenranta University of Technology, Fin-53851, Lappeenranta, Finland
(Received 9 March 1999)

At high solid concentrations, computer simulations of sheared granular materials comprised of randomly arranged, monodisperse, smooth, inelastic spherical particles flowing in a Couette geometry show large fluctuations in the normal stress at the walls. These fluctuations are characterized by a marked asymmetric amplitude distribution similar to those observed in recent experiments. In these systems the particles' mean square displacement in the shear direction is observed to vanish locally which indicates the formation of crystallized regions. However, there are other regions in the system with nonzero values for the mean square displacement in the shear direction. This observation indicates that a sheared monodisperse granular material initially in a disordered state could evolve to a system in which the crystal phase is formed largely with a well-defined interface between different phases. The periodic phase transition is observed between the compressed, highly ordered crystalline state and the dilated, less ordered state of the layer of particles adjacent to the wall, which may explain the stick-slip behavior which occurred in the experiments.
[S1063-651X(99)05612-3]

PACS number(s): 45.70.Mg, 61.20.Ja, 83.50.−v

I. INTRODUCTION

The interest in granular flows, such as grain flow in silos [1], catalytic particle flow in beds [2], rockfalls [3], and pack-ice flows [4], arises because granular flows exhibit a wide range of rheological behavior related to the kinds of interactions that take place between grains. It appears that many real engineering problems, such as applications to the industrial handling, are in a flow regime involving instantaneous collisions between the grains as well as long lived sliding contacts [5]. In contrast, there is clear experimental evidence [6] that the dynamics of grains may be dominated by collisions rather than sliding contacts even in slow dense flows. Therefore, the physical relevance of the assumption that grains in a dense flow have complex interactions of finite duration [7] remains a topic of controversy.

The motivation for this study is, therefore, to examine carefully the importance of particle surface roughness in describing the observed dynamical features of continuously sheared granular materials at high solid concentrations [8]. To this end, computer simulations based on the model described in Sec. II are used to produce results suitable for comparison with available experimental data. Simulations of shearing flows of randomly arranged, monodisperse, spherical particles with rough or smooth surfaces were carried out in a Couette geometry. The results of simulations are presented in Sec. III. The time series of the dimensionless normal stress at the walls revealed the presence of stick-slip dynamics in the shearing flows of a system comprised of smooth particles at solid volume fraction of 0.6, where a crystalline phase is formed which spans a large part of the computational box. The present results are of interest since they may motivate new theoretical efforts toward understanding the microscopic origin of stick-slip behavior.

II. SIMULATION MODEL

One possible method for the simulation of granular assemblies under shear is the soft sphere molecular dynamics approach in which each particle during a collision interacts with its neighbors by a damped normal force, which is a function of the degree of deformation at points of contact, as well as a superimposed shear force, which is simply related to the normal force by introducing a coefficient friction μ [9]. In this time-driven simulation, to assure sufficient accuracy, the interaction force between the particles must be calculated at least 100 times due to the presence of a very large gradient of the interaction force during a collision. Therefore, a three-dimensional simulation with a large number of particles may not currently be achievable using this approach.

It has been assumed previously that an event-driven simulation algorithm can be used for the simulation of a dense granular flow in which the effect of friction may be of interest [10]. The algorithm allows the creation of the trajectories of a large number of particles in the simulation box by calculating only the precollisional and postcollisional velocities and spins, without considering the details of the collision.

Given that previous models [10,11] do not provide the details of the collisions, an obvious question is how could these types of models be used to study the frictional effects. To address this question, a brief discussion of the present model is given below.

In the present study, the hard-sphere model of Alder and

Wainwright [12] has been modified by introducing dissipation through a coefficient of restitution e, which is proportionality relation between the precollisional and postcollisional normal impact velocities in a binary collisiion. That is,

$$(\mathbf{V}_{12}^{\mathrm{imp}\prime}\cdot\hat{\mathbf{k}})\hat{\mathbf{k}}=-e(\mathbf{V}_{12}^{\mathrm{imp}}\cdot\hat{\mathbf{k}})\hat{\mathbf{k}}, \tag{1}$$

where the impact velocity, which is the relative velocity of the two points on the particle surfaces that come together at impact, $\mathbf{V}_{12}^{\mathrm{imp}}$, is given by

$$\mathbf{V}_{12}^{\mathrm{imp}}=(\mathbf{V}_1-\mathbf{V}_2)-\frac{\sigma}{2}\hat{\mathbf{k}}\times(\omega_1+\omega_2). \tag{2}$$

Here σ is the diameter of the particle, $\mathbf{V}_i$ and ω_i are the translational velocity of the center and the spin of i^{th} particle $(i=1,2)$, respectively, $\hat{\mathbf{k}}$ is the unit vector directed from the center of particle 1 to that of particle 2 at the moment of impact, and the prime indicates the post-collisional value of the relative velocity, $\mathbf{V}_{12}^{\mathrm{imp}}$.

Measurements have shown that the normal restitution coefficient e, which depends significantly on the impact velocity, decreases from unity as the normal impact velocity, which is the component in the direction of $\hat{\mathbf{k}}$, namely, $V_n=\mathbf{V}_{12}{}^{\mathrm{imp}}\cdot\mathbf{k}$, increases from zero [13]. Assuming that the collisions are slow enough so that no plastic deformation occurs, Schwager and Poschel [14] used a generalization of the Hertz theory of elastic impact for the case of viscoelastic collisions and suggested an approximate functional form for $e(V_n)$ as $1-e\sim V_n^{1/5}$, which appears to be in agreement with the experimental data. Following Schwager and Poschel, the heuristic functional form for the coefficient of restitution is assumed given by

$$e(V_n)=1-(1-e)(V_n/V_0)^{1/5}. \tag{3}$$

Here e and V_0 are the adjustable parameters of the model used to obtain a fit to the data, where V_0 has the same dimension as V_n.

As the two rough particles collide, not only the normal component but also the component of $\mathbf{V}_{12}^{\mathrm{imp}}$ in the direction perpendicular to $\hat{\mathbf{k}}$, namely, $\hat{\mathbf{k}}\times(\mathbf{V}_{12}^{\mathrm{imp}}\times\hat{\mathbf{k}})$, is changed such that

$$\hat{\mathbf{k}}\times(\mathbf{V}_{12}^{\mathrm{imp}\prime}\times\hat{\mathbf{k}})=-\beta\hat{\mathbf{k}}\times(\mathbf{V}_{12}^{\mathrm{imp}}\times\hat{\mathbf{k}}), \tag{4}$$

where β is the tangential coefficient of restitution.

In the present idealized model, the value of β depends on the surface friction coefficient μ, as well as the ratio of the normal impulse, $m\eta_1(\hat{\mathbf{k}}\cdot\mathbf{V}_{12}^{\mathrm{imp}})\hat{\mathbf{k}}$, and the tangential impulse in the direction perpendicular to $\hat{\mathbf{k}}$ and lies in the plane of $\hat{\mathbf{k}}$, namely, $m\eta_2\hat{\mathbf{k}}\times(\mathbf{V}_{12}^{\mathrm{imp}}\times\hat{\mathbf{k}})$.

Assuming that slipping and sticking regions do not coexist in a given impact and the normal and tangential impulses at point of contact obey the Coulomb law of friction, it can be stated that if $\eta_2|\hat{\mathbf{k}}\times(\mathbf{V}_{12}^{\mathrm{imp}}\times\hat{\mathbf{k}})|=\mu\eta_1|(\hat{\mathbf{k}}\cdot\mathbf{V}_{12}^{\mathrm{imp}})\hat{\mathbf{k}}|$, the particle surfaces slip over one another and, therefore, the tangential coefficient of restitution is found as

$$\beta=-1+\mu(1+e)(1+1/K)|(\hat{\mathbf{k}}\cdot\mathbf{V}_{12}^{\mathrm{imp}})\hat{\mathbf{k}}|/|\hat{\mathbf{k}}\times(\mathbf{V}_{12}^{\mathrm{imp}}\times\hat{\mathbf{k}})|. \tag{5}$$

Otherwise, if $\eta_2|\hat{\mathbf{k}}\times(\mathbf{V}_{12}^{\mathrm{imp}}\times\hat{\mathbf{k}})|<\mu\eta_1|(\hat{\mathbf{k}}\cdot\mathbf{V}_{12}^{\mathrm{imp}})\hat{\mathbf{k}}|$, sticking or nonslipping contact is assumed to occur. This is a rather intriguing phenomena which involves not only the reduction of the magnitude of the relative velocity in the tangential but also the reversal of its direction during a collision. For this case, the value of the tangential coefficient of restitution may be assumed to be that suggested in Ref. [10], which is a phenomenological constant characterizing the restitution of velocity in the tangential direction for sticking contact, denoted by β_0. In the above, $\eta_1=\frac{1}{2}(1+e)$, $\eta_2=\frac{1}{2}(1+\beta)K/(1+K)$, and $K=4I/(m\sigma^2)$, and m and I are the mass and the moment of inertia of the particle, respectively.

The special case of $\beta=0$ which is used in the previous simulations [11] corresponds to situations in which phenomenological parameters, namely, inelasticity and surface friction, are sufficient to eliminate the postcollisional relative velocities in the tangential direction.

Once the coefficients of restitution have been calculated, the postcollisional velocities and spins, which are required in order to create the particles trajectories in the cell, can be determined using the following expressions obtained by the consideration of the conservation of momentum in a binary collision:

$$\mathbf{V}_1-\mathbf{V}_1'=\mathbf{V}_2'-\mathbf{V}_2=(\eta_1-\eta_2)(\hat{\mathbf{k}}\cdot\mathbf{V}_{12}^{\mathrm{imp}})\hat{\mathbf{k}}+\eta_2\mathbf{V}_{12}^{\mathrm{imp}}, \tag{6}$$

$$\omega_1'-\omega_1=\omega_2'-\omega_2=\frac{2\hat{\mathbf{k}}}{K\sigma}\times[\eta_2\hat{\mathbf{k}}\times(\mathbf{V}_{12}^{\mathrm{imp}}\times\hat{\mathbf{k}})].$$

Using the details mentioned above, simulations of shear flows of a granular material were carried out on systems comprised of 4296 of randomly arranged, monodisperse, spherical particles in periodically repeated rectangular cells. The particles are driven into shearing flow by moving the top and bottom walls in opposite directions along the x direction. The walls are made up of two irregular cubic arrays comprised of 400 very massive hemispherical particles with the same diameter as the interior particles. The computational box is rectangular, and the lengths of the box in the direction of the local velocity, the shear, and the direction normal to both the local velocity and shear, are $L_x=1$, $L_z=0.497$, and $L_y=1$, respectively. The initial velocities are assigned random directions with a magnitude according to a linear velocity profile $\mathbf{U}(z)=\gamma z\mathbf{e}_x$. The initial spins are all set to zero. Here $\mathbf{U}(z)$ is the axial velocity, γ is the apparent shear, and $\mathbf{e}_x$ represents the unit vector in the x direction, which is the direction of mean flow. Further details including a geometrical description of the problem were presented in previous studies [15].

III. RESULTS AND DISCUSSION

In this section attempts are directed toward finding appropriate values for the phenomenological parameters of the model discussed in Sec. II by which the observed macroscopic flow features [8] can be predicted for a sheared granu-

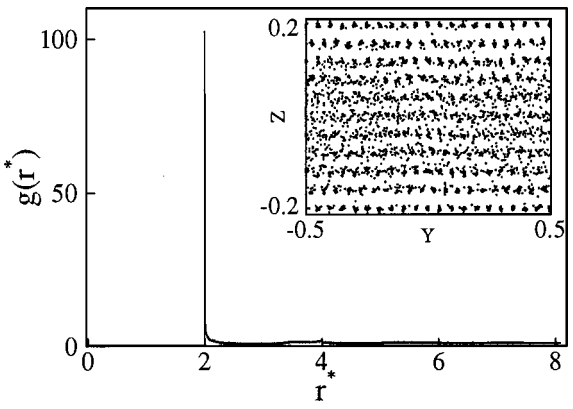

FIG. 1. Radial distribution function of a sample taken after about 5×10^7 collisions, for $\bar{\phi}_s\approx0.6$, $e=0.84$, $\mu=0.41$, and $\beta_0=0$. Here $r^*=r/R$, where r is a distance. Inset: Projection of particles positions in the sample onto the plane (yz). In this figure, and in Fig. 9 only the center points of the particles are shown.

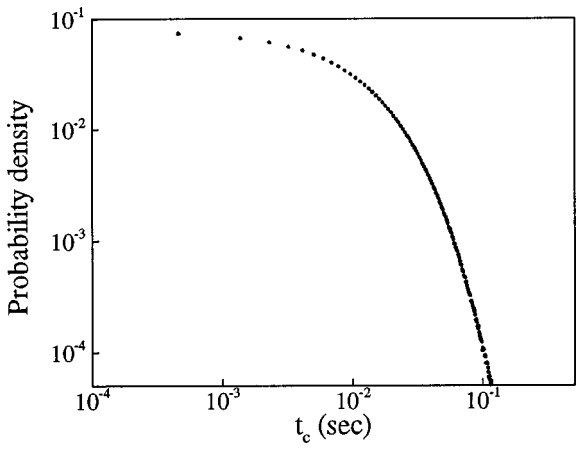

FIG. 2. The probability that a particle survives a time t_c without suffering a collision. The solid volume fraction is $\bar{\phi}_s\approx0.565$, and the phenomenological parameters are those of Fig. 1.

lar flow. Here the surface roughness is characterized by a coefficient of friction μ, as well as a phenomenological constant for sticking contact, β_0. It should be noted that the values of the particle phenomenological parameters e, μ, and β_0 for collisions between interior particles and wall particles are taken to be the same as those for collisions between interior particles. The extreme case with surface friction coefficient $\mu=0$ might resemble the shearing flow in which the dynamics of grains is dominated by collisions. In the other extreme case, where the particle surface is assumed to be quite rough, namely, $\mu=0.41$ [16], the frictional contact force between the particles governs the flow dynamics and collisional effects are of minor relevance.

By increasing the apparent shear rate from zero to $\gamma=2U/L_z\approx4\ \mathrm{s}^{-1}$, which falls toward the upper end of the range of shear rate of the experiments [8], a shear flow is applied to the system described in Sec. II which is comprised of randomly arranged, rough, inelastic spherical particles at a solid volume fraction of 0.6. Here U represents the velocity of one of the walls. Dissipation generated by particle-particle collisions is modeled using a constant coefficient of restitution, $e=0.84$, as well as a surface friction coefficient $\mu=0.41$. The phenomenological constant for sticking contacts, β_0, is set to zero. Therefore, the selected values of the phenomenological parameters are close to those used in the previous simulations [11]. The radial distribution function of a sample taken after 5×10^7 collisions is shown in Fig. 1. The value of the radial distribution function at contact implies that the mean free time between collisions should be very short. From the results obtained, the mean free time for an individual particle was calculated to be about 8×10^{-7} sec. Therefore, at a high solid volume fraction with the selected phenomenological parameters, the system hardly can be considered as shearable.

It is instructive to consider how decreasing the solid volume fraction can change the mean free time. By decreasing the average solid volume fraction to 0.565, with the same phenomenological parameters as mentioned above, the mean free time increases to 0.015 sec, which is about two orders of magnitude higher than the typical value of the duration of a collision [13]. As shown in Fig. 2, the probability that a particle experiences a collision less than 10^{-3} sec after its previous collision is quite small. Based on this observation the use of the idealized dissipative hard-sphere model described in Sec. II seems to be justified. However, it is necessary at this point to examine the variation of dimensionless normal stress, $P^*=P/[4\rho_pR^2(2U/L_z)^2]$, on the wall with dimensionless time, $t^*=tU/L_z$, as shown in Fig. 3. Here t represents time, ρ_p is the material density, and R is the particle radius. Since the localized time-dependent stresses have been found experimentally to be far larger than the mean [8], it can be concluded that the simulations performed using the above-mentioned values of the particle surface properties are not fully representative of real granular systems.

The theory of Lun and Savage [17] revealed that in a similar shearing motion, particles with rough surfaces could have more energy in rotational mode than particles with smooth surfaces. In this light, the shearing motion of a system of spherical particles with surfaces smoother than those in the above-mentioned simulations could provide the translational fluctuation energy needed for the large scale fluctua-

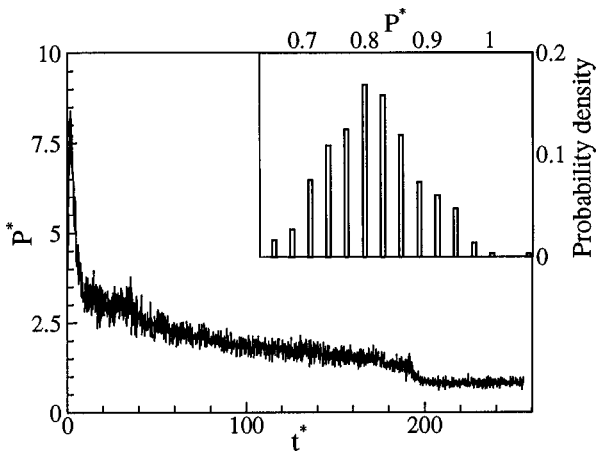

FIG. 3. Dimensionless normal stress P^*, exerted on the wall, vs dimensionless time t^* for $\bar{\phi}_s\approx0.565$, $e=0.84$, $\mu=0.41$, and $\beta_0=0$. Inset: The probability density function of the dimensionless normal stress at $t^*>200$, where the mean dimensionless normal stress is a constant, namely, $\overline{P^*}=0.81$.

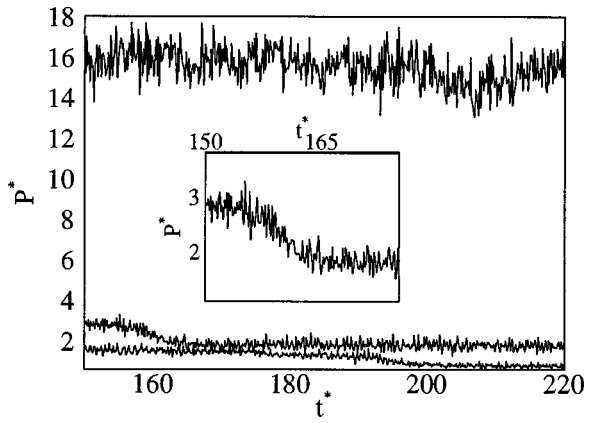

FIG. 4. Dimensionless normal stress P^* vs dimensionless time t^*; the upper curve is for $\bar{\phi}_s \approx 0.565$, $e=0.93$, $\mu=0$ (particles with smooth surfaces); the curve in the middle is for $\bar{\phi}_s \approx 0.565$, $e=0.93$, $\mu=0.123$, and $\beta_0=0.4$; and the lower curve is a portion of Fig. 3. Inset: Portion of the middle curve where a significant change in the dimensionless normal stress can be seen at $150 \leqslant t^* \leqslant 165$.

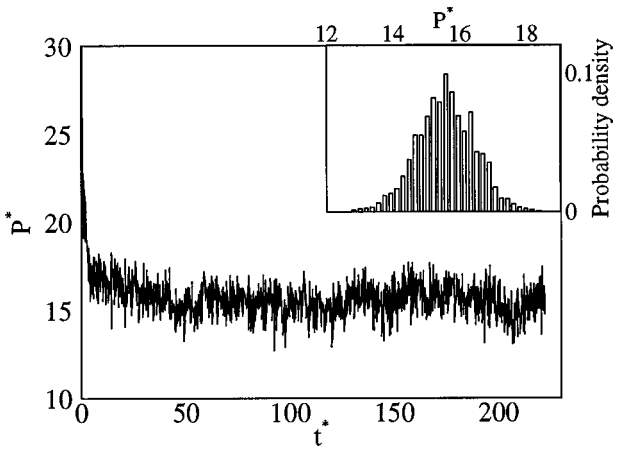

FIG. 5. Dimensionless normal stress P^* exerted on the wall vs dimensionless time t^*, for smooth inelastic particles for $e=0.93$ at a solid volume fraction of $\bar{\phi}_s \approx 0.565$. Inset: The probability density function of the dimensionless normal stress at $50 < t^* < 220$.

tions observed experimentally [8]. To test this hypothesis, the values for the phenomenological parameters suggested by Lun and Bent [10] for steel balls are used, namely, the coefficient of restitution $e=0.93$, the surface friction coefficient $\mu=0.123$, and the phenomenological constant for sticking contact $\beta_0=0.4$. At a solid concentration of 0.565, convincing evidence supporting the aforementioned theory is found by considering the large scale of fluctuations occurring when smooth particles, whose surface friction coefficient is zero, were used in simulations. This is illustrated in Fig. 4, which compares the dimensionless normal stress on the wall of cases at the same average solid volume fractions and average shear rates, but with different phenomenological parameters. There are sudden decreases in dimensionless normal stress in the shearing flow of rough particles, as shown in the inset of Fig. 4. However, in general the results support the notion that the rough particles tend to have more energy in rotational mode than smooth particles.

Comparing the results presented in Fig. 4 with those of real systems [8], it appears even more certain that the dynamics of grains could be dominated by collisions rather than sliding contacts in dense flows of granular materials under continuous shear. But the simulation result for particles with smooth surfaces at a solid volume fraction of 0.565 still shows a discrepancy in flow behavior vis-a-vis that of real systems. Recent annular shear cell tests [8] revealed a marked asymmetric shape in the amplitude distribution. In this case, the fluctuations seem to be symmetric around a mean value, as depicted in Fig. 5.

At this stage, it is natural to ponder why such a disagreement should occur. The explanation appears to lie with the value of solid volume fraction in the above-mentioned simulation. As shown in Fig. 6, at a solid volume fraction of 0.6, fluctuations in time series of the dimensionless normal wall stress, which are obtained for a system of monodisperse, smooth spherical particles with a coefficient of restitution $e=0.93$, show a strong analogy with those observed in recent experiments [8].

Considering the profound differences in the time series for the dimensionless normal stresses illustrated in Figs. 5 and 6, there is concern as to whether the system at higher solid volume fraction, namely, 0.6, behaves as a fluid. Generally, the radial distribution function $g(r^*)$ is used to distinguish fluidlike from solidlike behavior [18]. Examining the radial distribution function for a sample taken from the system at solid volume fraction of $\bar{\phi}_s=0.6$, as shown by dashed line in Fig. 7, an additional peak can be observed between the first- and second-nearest-neighbor peaks. This behavior of the radial distribution function is very different from that of the fluidlike system at a solid volume fraction of 0.565, denoted in Fig. 7 by a solid line. Therefore, there is a clear indication that the initially disordered sample at a solid fraction of 0.6, had partially crystallized under shearing motion.

At this stage it is interesting to examine the fluctuations, as shown in Fig. 6, by considering the power spectra of the time series for the dimensionless normal stress about the mean value. As seen from Fig. 8(a), the power density ap-

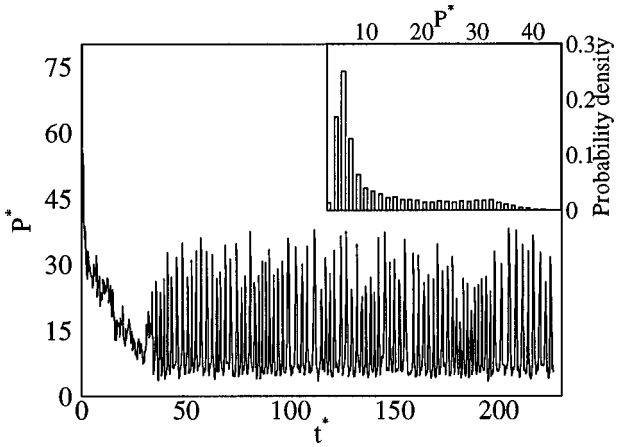

FIG. 6. Dimensionless normal stress P^*, exerted on the wall, vs dimensionless time t^*, for smooth inelastic particles for $e=0.93$ at solid volume fraction of $\bar{\phi} \approx 0.6$. To provide a better visualization, only every 20th point is plotted. Inset: The probability density function of the dimensionless normal stress at $50 < t^* < 220$, where the mean dimensionless normal stress is a constant, namely, $\bar{P} \approx 11.5$.

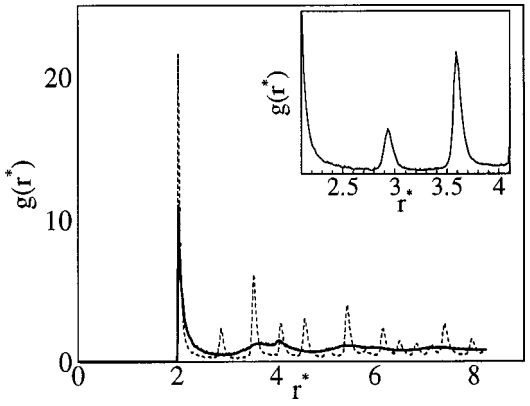

FIG. 7. The dashed line is the radial distribution function of a sample taken after $t^* \approx 150$, for smooth inelastic particles for $e = 0.93$ at a solid volume fraction of $\bar{\phi}_s \approx 0.6$. Inset: Fewer particle pairs separated by 2.8, but more pairs separated by 3.5. The solid line represents the radial distribution function of a sample taken after $t^* \approx 150$, for smooth inelastic particles for $e = 0.93$ at a solid volume fraction of $\bar{\phi}_s \approx 0.565$. No indication of the crystalline structure can be observed.

pears to be a function of an inverse power of frequency at low frequencies, and the spectra become even steeper at high frequencies ($f > 30$ Hz). Unfortunately, the use of a discrete Fourier transform does not generate a smooth power spectrum density. Therefore, the straight lines which indicate the power laws of $f^{-0.6}$ and f^{-2} which represents the scaling behavior of data [8] at low and high frequencies, respectively, are also plotted in Fig. 8(a) for the comparison. It is worth mentioning that the relatively smooth power spectra illustrated in Ref. 8 were obtained using a Hamming window [19].

There is, however, a significant difference between the behavior of the spectra as illustrated in Fig. 8(a) and those of Miller, O'Hern, and Behringer [8] at the intermediate range of $4 < f < 25$. The characteristic harmonic frequencies can be observed in Fig. 8(a), which may be associated with the stick-slip motion observed by Hanes and Inman [20]. To provide a better visualization of these frequencies, a short-term Fourier transform is used, which consists of computing the Fourier coefficients of the product of dimensionless normal stress within the interval $50 < t^* < 150$ and a sliding compactly supported window function [21]. Figure 8(b) illustrates the spectrogram of a sequence of the magnitude of the time-dependent Fourier transform versus time. These frequencies are long lived, and the slight change of frequency with time might be related to some dynamical instability in the system.

In the present system, stick-slip motion may be associated with the periodic phase transition between the compressed, highly ordered state and the dilated, less ordered state of the thin layer of particles separating the moving upper wall from a crystallized region, as shown in Fig. 9. It can easily be visually discerned that the crystallized region is located at $(-0.5,0.5) \times (0,0.18)$ and the aforementioned thin layer at $(-0.5,0.5) \times (0.2,0.22)$. It would be useful, however, to obtain a more quantitative measure of the symmetry of clusters comprised of a particle and its 12 nearest neighbors in the crystallized region. To this end a set of orientational order

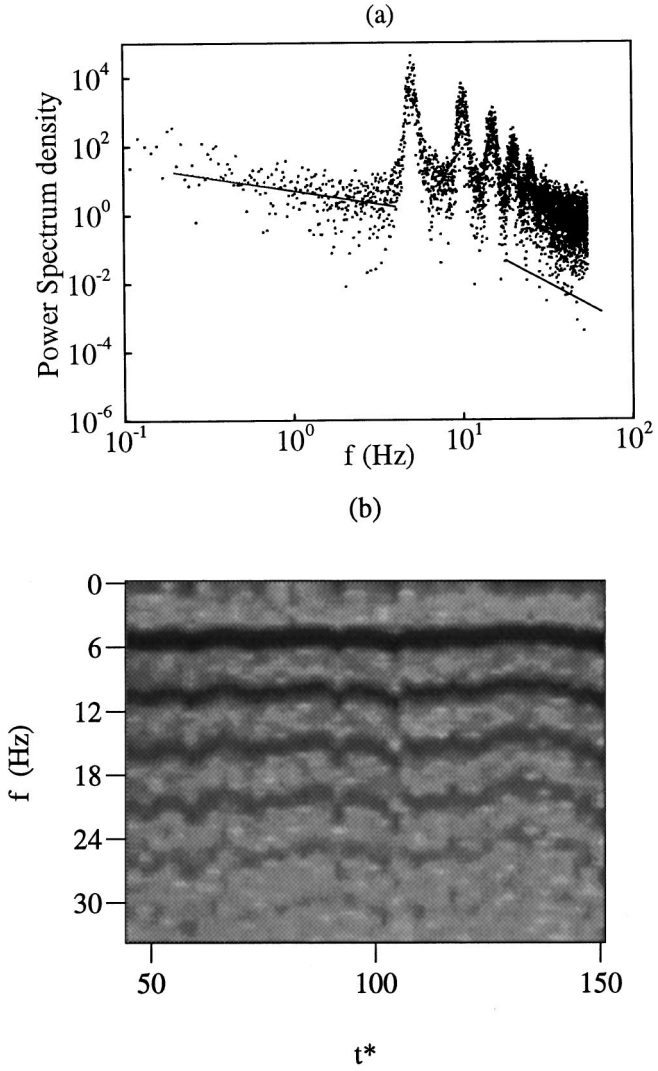

FIG. 8. (a) The power spectrum of the steady state portion of the time series for dimensionless normal stress shown in Fig. 6. The straight lines at the left and the right indicate the power laws $f^{-0.6}$ and f^{-2}, respectively. (b) Short-time Fourier transform. Shown is the magnitude of the time-dependent Fourier transform of the portion of time series at $50 < t^* < 150$. Only a portion of the frequency domain, namely, $4 < f < 30$, is shown. The magnitude intensity is coded using a gray scale, from white (low intensity) to black (high intensity).

parameters, denoted by $Q_{lm}(\mathbf{R}) \equiv Y_{lm}(\theta(\mathbf{R}), \phi(\mathbf{R}))$, is associated with each bond which joins a particle with its near neighbors [22]. For the crystalline region, the reduced rotationally invariant combinations of Q_{lm}, namely,

$$\hat{W}_l \equiv \frac{\sum_{\substack{m_1,m_2,m_3 \\ m_1+m_2+m_3=0}} \begin{pmatrix} l & l & l \\ m_1 & m_2 & m_3 \end{pmatrix} \bar{Q}_{lm_1} \bar{Q}_{lm_2} \bar{Q}_{lm_3}}{\left[\sum_m |Q_{lm}|^2 \right]^{3/2}}, \quad (7)$$

are found to be $\hat{W}_4 = -0.135$, $\hat{W}_6 = -0.013$, $\hat{W}_8 = 0.057$, and $\hat{W}_{10} = 0.036$. Except for a sign of $\hat{W}_{10}$, the values of $\hat{W}_l$ are consistent with cuboctahedral symmetry [22]. Here $\mathbf{R}$ represents the position of the bond midpoint,

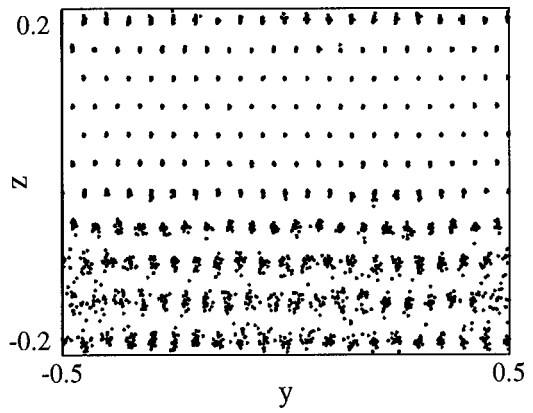

FIG. 9. Projection of particles positions onto the plane (y,z). The values of solid volume fraction and the phenomenological parameters are those of Fig. 6.

$Y_{lm}(\theta(\mathbf{R}),\phi(\mathbf{R}))$ are spherical harmonics, $\theta(\mathbf{R})$ and $\phi(\mathbf{R})$ are the polar angles of the bond measured with respect to a fixed reference coordinate system, the coefficients

$$\begin{pmatrix} l & l & l \\ m_1 & m_2 & m_3 \end{pmatrix} \tag{8}$$

are Wigner $3j$ symbols, and the averaged quantity $\overline{Q}_{lm} \equiv \langle Q_{lm}(\mathbf{R}) \rangle$ is taken over the bonds joining particles in the sample with their near neighbors.

Another quantity that can be used to distinguish fluid from solid-like behavior is the mean square displacement defined by

$$\langle \Delta Z^{*2} \rangle = N^{-1} \sum_{i=l}^{N} \langle [Z_i^*(t^*+\tau^*) - Z_i^*(t^*)]^2 \rangle. \tag{9}$$

Here $Z_i^*(t^*) = Z_i(t^*)/(2R)$ represents the position of particle i in the z direction at dimensionless time t^*, which is normalized by the particle diameter; N is the number of particles in the computational box; t is time, $\tau^* = \tau U/L_z$ shows that the samples are taken a time interval τ apart; and the angular brackets indicate the ensemble average.

As can be seen in Fig. 10, particles with smooth surfaces are diffusive, except for those particles located in the crystalline region. This is consistent with recent experimental observations [23] for which movement of the particles in directions transverse to the bulk motion were reported at a very high solid concentration. The particle movements in the direction normal to the shear plane in this system can be caused by several thermodynamic forces [24]. Therefore, it is not clear that the self-diffusion coefficient can be deduced from data shown in Fig. 10 using the Einstein relation [25]. This *ad hoc* method suggested in Ref. [23], which was also used in an earlier work [26], can at best result in an effective particle diffusion coefficient.

Efforts at understanding the particle diffusive motion in the above-mentioned system resulted in finding the presence of a two phase granular flow, in which solid and liquid phases coexist, in the computational box. A streamline in the noncrystalline region [27], as shown in the inset of Fig. 10, exhibits a behavior which indicates the presence of large, slow fluctuations. A study of phase transformation as well as the implications of phase coexistence in dense granular flows are planned to be discussed in a subsequent paper.

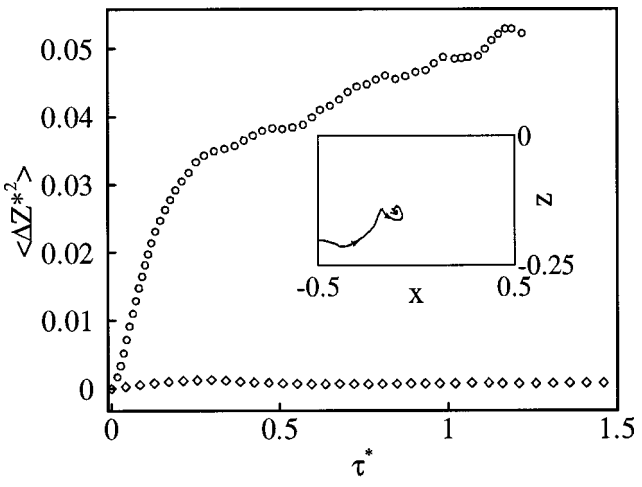

FIG. 10. Variations of dimensionless mean square displacement, $\langle \Delta Z^{*2} \rangle$, with τ^*. The circles and diamonds represent the calculated value of $\langle \Delta Z^{*2} \rangle$ for the noncrystalline and crystalline regions, respectively, of the configuration shown in Fig. 9. Inset: A streamline in the noncrystalline region of the configuration shown in Fig. 9.

In order to validate the premise that collisions rather than sliding contact may dominate the dynamics of dense granular flows, different values of particle phenomenological parameters should be considered. As such, simulations were run to examine the effect of surface roughness on the dynamics of grains at high solid volume fractions. Figure 11 clearly illustrates that at a solid volume fraction of 0.6, the fluctuations in the time series for the normal stress of the shear flow of inelastic frictional spherical particles—with the phenomenological parameters $e=0.93$, $\mu=0.123$, and $\beta_0=0.4$—are symmetric around a mean value. Therefore, in the absence of granular crystals, granular materials flowing in a Couette geometry do not show a wall normal stress signature similar to

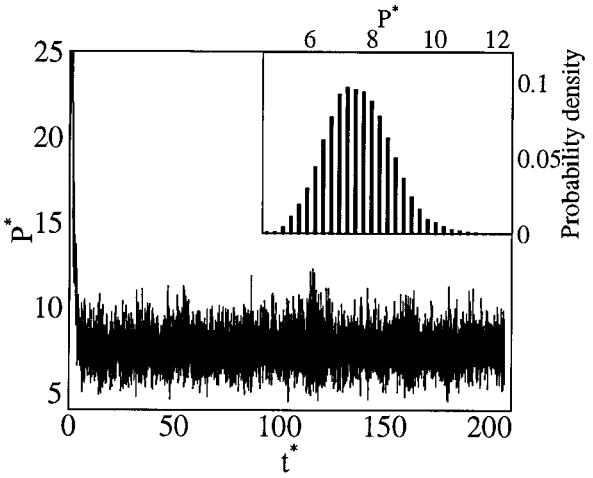

FIG. 11. Dimensionless normal stress P^* vs dimensionless time t^*, for rough, inelastic particles for $\overline{\phi}_s \approx 0.6$, $e=0.93$, $\mu=0.123$, and $\beta_0=0.4$. Inset: The probability density function of the dimensionless normal stress at $20<t^*<200$, where the mean dimensionless normal stress is a constant, namely, $\overline{P}^* \approx 7.6$.

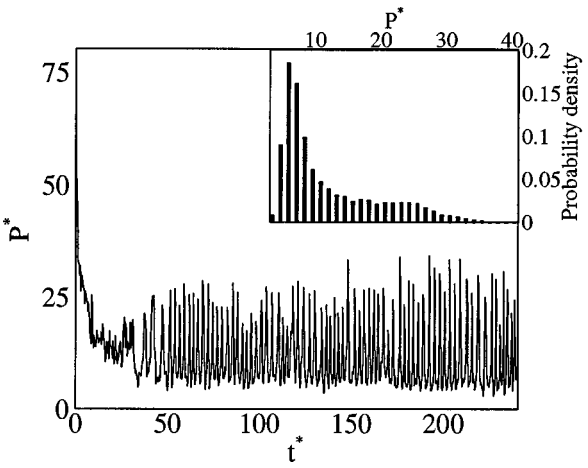

FIG. 12. Dimensionless normal stress P^* vs dimensionless time t^*, for smooth inelastic particles for $e(V_n)=1-(1-e)(V_n/V_0)^{1/5}$. The model parameters are $e=0.93$ and $V_0=0.5$. To provide a better visualization, only every 20th point is plotted. Inset: The probability density function of the dimensionless normal stress at $70<t^*<240$.

that observed in recent experiments [8]. This observation, which supports the earlier conjecture that the microscopic origin of stick-slip behavior could be the shear-melting transitions and recrystallization of the layer of particles adjacent to the wall, provides further evidence that the dynamics of dense granular flows may be collision dominated.

However, the results presented above using a constant coefficient of restitution may be regarded with some suspicion, since measurements have shown that the normal restitution coefficient is not a constant, and that it depends significantly on the impact velocity [10]. To examine the effect of a coefficient of restitution, which depends on the normal impact velocity on the dynamics of grains, Eq. (3) with $V_0=0.5$ is used. This heuristic model can predict the trend of data well [10]. However, the value of the constant e in the model is chosen to be that suggested in the above, namely, 0.93, by which the large scale fluctuations observed in the real system [8] can be generated. Simulations for $e=0.93$ and $V_0=0.5$ resulted in somewhat similar time series for the dimensionless normal wall stress, as shown in Fig. 12. Comparing the results presented in Figs. 6 and 12 with those of real systems [8], the effect of a velocity-dependent coefficient of restitution on the dynamics of grains may not be pronounced for the flow conditions considered in this study. However, the large scale fluctuations, as shown in Fig. 12, seem to be closer to what was observed experimentally [8].

IV. CONCLUSIONS

Computer simulations with an idealized collisional model were performed for both smooth and rough, monodisperse spherical particles in a Couette flow to examine the effect of particle phenomenological parameters on the flow dynamics. When smooth particles were used, an asymmetric normal stress distribution at the wall was obtained, consistent with recent experimental findings [8]. In addition, for this case crystallization was observed to occur, as characterized by the local absence of diffusion, although diffusion still existed in the noncrystallized regions. Significantly, by examining the fluctuations of the normal stress on the walls, the presence of the stick-slip motion was found in this system. This finding may explain the unsteady complications which occurred in the experiments of Hanes and Inman [20]. The origin of stick-slip behavior appears to be the shear-induced melting and recrystallization of the layer of particles adjacent to the wall. In light of the findings of the present study, future theoretical studies will be conducted with the goal of improving our understanding of the microscopic origin of stick-slip behavior. Comparing the results of the simulations with previously reported experimental data, it can be concluded that the present idealized collisional model can predict the experimental observations quite closely.

ACKNOWLEDGMENT

The authors are grateful to Professor Robert P. Behringer at Duke University for helpful discussions.

[1] P. Claudin and J.P. Bouchaud, Phys. Rev. Lett. **78**, 231 (1997).
[2] D. Kunii and O. Levenspiel, *Fluidization Engineering* (Butterworth-Heinemann, Boston, 1991).
[3] T. H. Erismann, Rock Mech. **12**, 245 (1976).
[4] D. A. Rothrock, Annu. Rev. Earth Planet Sci. **3**, 317 (1975).
[5] P. C. Johnson and R. Jackson, J. Fluid Mech. **176**, 67 (1987).
[6] N. Menon and D. J. Durian, Science **275**, 1920 (1997).
[7] S. B. Savage, in *Physics of Granular Media*, edited by D. Bideau and J. Dodds (Nova, New York, 1992).
[8] B. Miller, C. O'Hern, and R. P. Behringer, Phys. Rev. Lett. **77**, 3110 (1996).
[9] P. A. Cundall and O. D. L. Strack, Geotechnique **29**, 47 (1979); P. K. Haff and B. T. Werner, Powder Technol. **48**, 239 (1986); P. A. Thompson and G. S. Grest, Phys. Rev. Lett. **67**, 1751 (1991); M. A. Scherer, V. Buchholtz, T. Poschel, and I. Rehberg, Phys. Rev. E **54**, 4560 (1996).
[10] C. Bizon, M. D. Shattuck, J. B. Swift, W. D. McCormick, and H. L. Swinney, Phys. Rev. Lett. **80**, 57 (1998); C. K. K. Lun and A. A. Bent, J. Fluid Mech. **258**, 335 (1994).
[11] C. S. Campbell, J. Fluid Mech. **348**, 85 (1997).
[12] B. J. Alder and T. Wainwright, J. Chem. Phys. **31**, 459 (1959).
[13] W. Goldsmith, *Impact: The Theory and Physical Behavior of Colliding Solids* (Edward Arnold Ltd., London, 1960).
[14] T. Schwager and T. Poschel, Phys. Rev. E **57**, 650 (1998).
[15] P. Zamankhan, H. Vahedi Tafreshi, W. Polashenski, Jr., P. Sarkomaa, and C. L. Hyndman, J. Chem. Phys. **109**, 4487 (1998).
[16] T. G. Drake, J. Fluid Mech. **225**, 121 (1991).
[17] C. K. K. Lun and S. B. Savage, J. Appl. Mech. **54**, 47 (1987).
[18] M. P. Allen and D. J. Tildesley, *Computer Simulation of Liquids* (Clarendon, Oxford, 1997).
[19] R. P. Behringer (private communication).
[20] D. M. Hanes and D. L. Inman, J. Fluid Mech. **150**, 357 (1985).
[21] I. Daubechies, IEEE Trans. Inf. Theory **36**, 961 (1990).
[22] P. J. Steinhardt, D. R. Nelson, and M. Ronchetti, Phys. Rev. B **28**, 784 (1983).

[23] S. S. Hsiau and M. L. Hunt, J. Fluid Mech. **251**, 299 (1993); V. V. R. Natarajan, M. L. Hunt, and E. D. Taylor, *ibid.* **304**, 1 (1995).

[24] P. Zamankhan, Phys. Rev. E **52**, 4877 (1995); Piroz Zamankhan, Parsa Zamankhan, and W. Polashenski, Jr. (unpublished).

[25] A. Einstein, Ann. Phys. (Leipzig) **17**, 549 (1905).

[26] P. Zamankhan, W. Polashenski, Jr., H. Vahedi Tafreshi, A. Shakib Manesh, and P. Sarkomaa, Phys. Rev. E **58**, 5237 (1998).

[27] The method suggested by J. C. Davis [*Statistics and Data Analysis in Geology* (Wiley, New York, 1986)] is used to calculate the streamline shown in the inset of Fig. 10.